Electrochimica Acta 142 (2014) 307–316

Contents lists available at ScienceDirect

Electrochimica Acta

journal homepage: www.elsevier.com/locate/electacta

# Molybdenum carbide-based electrocatalysts for CO tolerance in proton exchange membrane fuel cell anodes

Ayaz Hassan [a], Valdecir Antonio Paganin [a], Alejo Carreras [b], Edson Antonio Ticianelli [a,*]

[a] Instituto de Química de São Carlos, Universidade de São Paulo, Caixa Postal 780, São Carlos, SP, CEP 13560-970, Brazil
[b] Instituto de Física Enrique Gaviola (IFEG)-CONICET, Facultad de Matemática, Astronomía y Física, Universidad Nacional de Córdoba, Medina Allende s/n, (5016) Córdoba, Argentina

ARTICLE INFO

*Article history:*
Received 21 May 2014
Received in revised form 16 July 2014
Accepted 22 July 2014
Available online 11 August 2014

*Keywords:*
Molybdenum carbide
PEMFC
Ultra-sonication
stability
CO tolerance

ABSTRACT

The activity, stability and CO tolerance of molybdenum carbide-based electrocatalyts were studied in anodes of proton exchange membrane fuel cells (PEMFCs). To this purpose, carbon-supported molybdenum carbide ($Mo_2C$/C) was prepared by an ultrasonic method, and was used as catalyst support in the anode of a PEMFC. Pt and PtMo nanoparticles were deposited on this $Mo_2C$/C by the formic acid reduction method. The physical properties of the resulting electrocatalysts were studied by X-ray diffraction (XRD), transmission electron microscopy (TEM), energy dispersive spectroscopy (EDS), X-ray absorption near edge structure (XANES), scanning electron microscopy (SEM) and wavelength dispersive spectroscopy (WDS). Electrochemical characterizations were carried out by single cell polarization measurements, CO stripping, cyclic voltammetry (CV) and online mass spectrometry (OLMS). CV and OLMS experiments were performed to evaluate the stability and CO tolerance of the electrocatalysts. The results obtained for the carbide-based electrocatalysts were compared with those obtained for carbon-supported PtMo and Pt electrocatalysts. It was observed that Pt and PtMo supported on $Mo_2C$/C present a better stability than PtMo supported on carbon. CV and WDS results evidenced a partial dissolution of Mo from the anode and its migration toward cathode during the cell operation. On the basis of polarization measurements and cyclic voltammograms, it was concluded that the stability of anode electrocatalysts can be improved by the use of molybdenum carbide as catalyst support.

© 2014 Elsevier Ltd. All rights reserved.

## 1. Introduction

Fuel cells are considered as alternative electrical power sources for the near future. Among the various types of fuel cells used today, the most promising is the proton exchange membrane fuel cell (PEMFC), which is particularly useful for portable applications, because of its relatively high power density despite the low temperature of operation [1]. The electrocatalysts most commonly used for hydrogen oxidation in the PEMFC anode mainly contain Pt, which ensures a good electrocatalytic activity. However, the hydrogen obtained from reformate fuel stream contains carbon monoxide (CO) impurities that are easily adsorbed on the Pt surface, thus reducing the Pt surface available for hydrogen adsorption and eventually reducing the cell performance [2]. Therefore, a transition metal such as Ru or Mo is typically added to the Pt in order to increase the CO tolerance of the anode electrocatalysts by desorbing CO molecules from Pt surface [3,4]. Unfortunately, the high price of these metals, particularly Pt and Ru, and wear of the catalysts, still prevent the large-scale commercialization of PEMFCs. Transition metal carbides have been studied because of their catalytic activities for many chemical reactions including hydrodenitrogenation, hydrodesulfurization, methanol steam reforming and water-gas shift (WGS) reactions [5,6]. These carbides can be produced having large surface area and catalytic properties resembling those of the Pt-group metals (PGMs) [7,8].

In particular, molybdenum carbide ($Mo_2C$) has been investigated as anode electrocatalyst for PEMFCs [9,10], although its catalytic activity for $H_2$ electro-oxidation is not high enough to meet the requirements for fuel cell applications [11]. However, the catalytic activity of this carbide can be noticeably improved by the addition of Pt. In a recent study conducted to evaluate the use of molybdenum carbide as electrocatalyst in fuel cell anodes, it has been reported that Pt-$Mo_{carb}$ supported on carbon black has shown a superior activity for methanol electro-oxidation in comparison with Pt supported on carbon [12]. In another study it was observed that molybdenum carbide has a high activity for the

* Corresponding author. Tel.: +55 16 3373 9945; fax: +55 16 3373 9952.
*E-mail address:* edsont@iqsc.usp.br (E.A. Ticianelli).

http://dx.doi.org/10.1016/j.electacta.2014.07.142
0013-4686/© 2014 Elsevier Ltd. All rights reserved.

dissociation of methanol and water, as well as a relatively low CO desorption temperature of around 330 K [13]. Moreover, Weigert et al. [9] observed that Pt-modified Mo-C has enhanced activity and stability compared to Pt supported on carbon.

Summarizing, some research data can be found in literature regarding the activity of $Mo_2C$/C either for methanol oxidation or oxygen reduction, however, the CO tolerance and stability of this material has not been studied in detail. Thus, in this work, molybdenum carbide was prepared and used as support of Pt and PtMo electrocatalysts for hydrogen electro-oxidation in the presence of 100 ppm CO in PEMFC anodes. In addition to physical and electrochemical properties, the stability of these electrocatalysts was studied, in comparison with carbon-supported PtMo and Pt electrocatalysts.

## 2. Experimental

### 2.1. Preparation of electrocatalysts

The molybdenum carbide support (30 wt%, $Mo_2C$/C) was prepared by sonicating a slurry of molybdenum hexacarbonyl ($Mo(CO)_6$, Aldrich) and carbon powder (Vulcan XC-72R) in hexadecane, with a high intensity ultrasonic horn at 90 °C for 3 h. The resulting mixture was filtered, washed several times with purified pentane and heated at 90 °C until a black powder was obtained. This powder was transferred to a tubular quartz reactor and placed in a furnace. It was then exposed to an argon flow at 100 °C during 1 h. The argon was then replaced by a 1:1 $CH_4/H_2$ mixture and the temperature was increased at a rate of 5 °C $min^{-1}$, firstly until 300 °C for 1 h, secondly until 400 °C also for 1 h and finally until 500 °C for 12 h, in order to carburize the black powder and obtain the molybdenum carbide [14,15]. Pt (20 wt%) was deposited on this carbide support by the formic acid reduction method [16–18], which consisted of the reduction of dihydrogen hexachloroplatinate hexahydrate ($H_2PtCl_6.6H_2O$, Aldrich), in the presence of the molybdenum carbide, using formic acid as reducing agent. In addition, PtMo (20 wt%) was deposited on $Mo_2C$/C and Vulcan XC-72R, also by the formic acid method. Pt supported on Vulcan XC-72 carbon also with 20 wt% metal/C was supplied by E-TEK. The Pt and PtMo loading in all the electrocatalysts was maintained at 20 wt%.

### 2.2. Physical characterizations

The metal content of the $Mo_2C$/C support as well as the metal loadings (Pt and Mo) of the catalysts were determined by energy dispersive x-ray spectroscopy (EDS) in a scanning electron microscope LEO, 440 SEM-EDX system (Leica-Zeiss, DSM-960) with a microanalyzer (Link analytical QX 2000) and a Si (Li) detector, using a 20 keV incident electron beam. The BET surface areas of the catalyst samples were determined by using a Micromeritics AutoChem II Chemisorption Analyzer. X-ray diffraction (XRD) patterns were recorded in a RIGAKU XRD RU200B diffractometer using CuKα radiation, in the 2θ range from 10 to 90°. Particle size distributions were determined by transmission electron microscopy (TEM, Tecnai G2F20 transmission electron microscope). The average crystallite sizes of the catalysts were determined by the Scherrer equation [19], using the Pt (220) diffraction peak and were compared with the results from TEM. The electronic properties of Pt in the electrocatalysts were investigated by x-ray absorption spectroscopy (XAS) (beamline D041 XAFS1 at the Brazilian Synchrotron Light Laboratory, LNLS) focused on the x-ray absorption near edge structure (XANES) region of the Pt $L_3$ absorption spectrum, that provides information about the electronic structure of the Pt 5d band and thus on the reactivity of the catalysts. These experiments were conducted by using a homemade spectro-electrochemical cell which

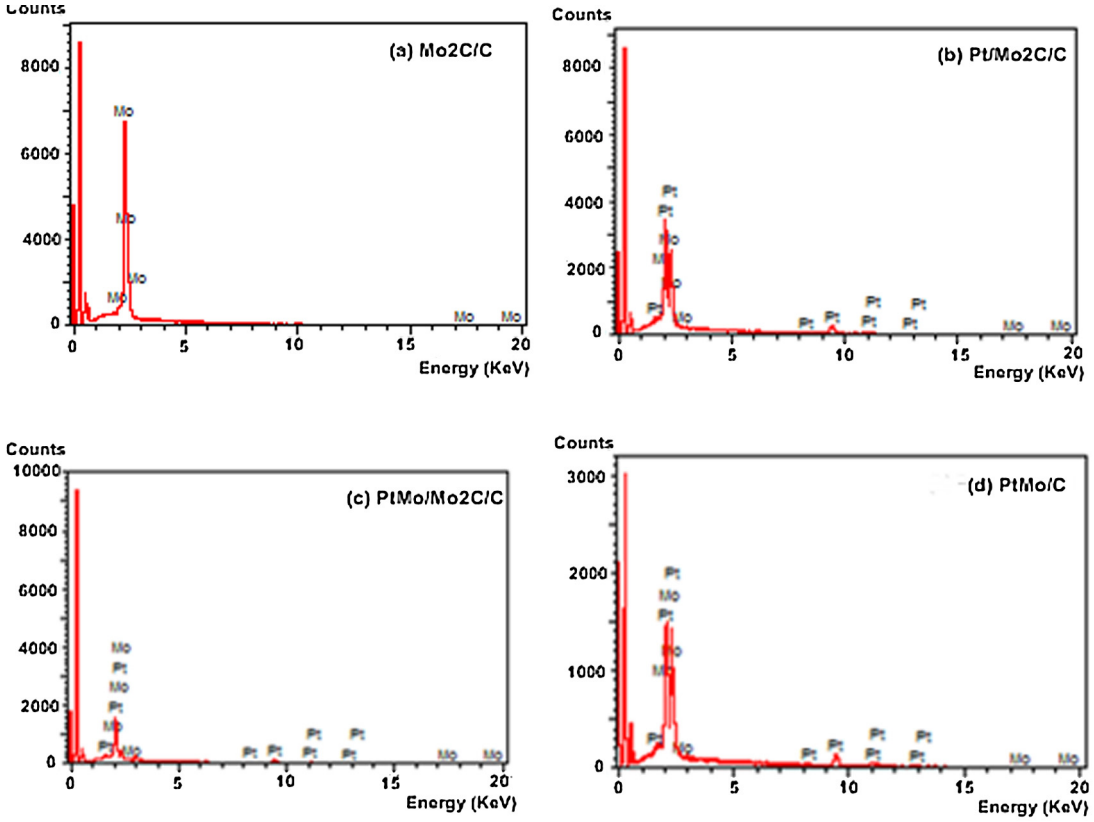


**Fig. 1.** EDS spectra of $Mo_2C$/C support and the Pt/$Mo_2C$/C, PtMo/$Mo_2C$/C and PtMo/C electrocatalysts.

**Table 1**
Chemical compositions, crystallite/particle sizes, lattice parameters and BET surface areas of the $Mo_2C$/C support and the Pt/$Mo_2C$/C, PtMo/$Mo_2C$/C and PtMo/C electrocatalysts.

| Electro- catalysts | Elements (wt%) determined by EDS | | | Pt crystallite/particle size (nm) | | Pt Lattice constant (A°) XRD | BET surface area ($m^2$/g) |
|---|---|---|---|---|---|---|---|
| | Pt (%) | Mo (%) | C (%) | XRD | TEM | | |
| $Mo_2C$/C | NA | 19.0 | 81.0 | NA | NA | NA | 113 |
| Pt/$Mo_2C$/C | 16.1 | 12.1 | 71.8 | 3.0 | 2.5 | 0.392 | 85 |
| PtMo/$Mo_2C$/C | 15.0 | 14.5 | 70.5 | 2.5 | 2.4 | 0.392 | 88 |
| PtMo/C | 13.3 | 3.0 | 83.7 | 2.4 | 2.5 | 0.391 | 190 |

enables to set virtually the same humidification, temperature and gas flux as in a fuel cell [20–22].

Scanning electron microscopy (SEM) and electron probe microanalysis (EPMA) of cross sections of the MEAs (membrane electrode assemblies) were performed, in order to investigate the loss of Mo from the anode electrocatalysts and its migration to the membrane and cathode. For this purpose, samples of the new and cycled MEAs were cut transversely with scissors, then they were mounted on aluminum sample holders, and finally they were coated with a carbon layer, in order to increase their surface electrical and thermal conductivities. SEM analysis was performed using a SIGMA (Carl Zeiss) field emission scanning electron microscope (FE-SEM), and EPMA analysis was done with a JEOL JXA 8230 electron probe microanalyzer, using a wavelength dispersive spectrometer and a PETJ analyzer crystal. SEM and EPMA experiments were carried out in the Laboratorio de Microscopía Electrónica y Análisis por Rayos X, from the Facultad de Matemática, Astronomía y Física (FAMAF), Universidad Nacional de Córdoba, Argentina.

### 2.3. Electrochemical measurements

The electrochemical measurements were conducted in a single cell, using membrane electrode assemblies (MEAs) prepared with Nafion membranes and electrodes formed by gas diffusion and catalyst layers. The metal load was 0.4 mg $cm^{-2}$ for the anodes (Pt/$Mo_2C$/C, PtMo/$Mo_2C$/C, PtMo/C and Pt/C) and cathode (Pt/C, E-TEK). The materials and method used for the preparation of MEAs and its components are described in detail elsewhere [16–18,20–22]. Fuel cell polarization measurements were carried out galvanostatically with the cell at 85 °C, using gases saturated with water at 100 °C for the anode and at 90 °C for the cathode. The system was first maintained at an initial potential of 0.7 V in pure $H_2$, for 2 h, and then at 0.8 V in $H_2$/100 ppm CO, also for 2 h, to reach the steady state before the data acquisition. CO stripping experiments were conducted at two different temperatures (25 and 85 °C), in order to study the CO tolerance of the prepared materials. These experiments were performed using a Solartron 1285 potentiostat/galvanostat in the standard fuel cell hardware. During the experiments the anode, used as working electrode, was either fed with Ar or CO (1000 ppm in Ar balance), while the cathode, used as both reference (reversible hydrogen electrode, RHE corrected approximately to 35 mV) and counter electrode, was constantly fed with $H_2$. The CO was firstly adsorbed on the anode for 30 minutes at a constant potential of 50 mV, and then the anode was flushed with Ar for another 30 minutes.

Online mass spectrometry analysis with $CO_2$ detection was conducted to study the oxidation of the CO adsorbed on the electrocatalyst surface. In these experiments the anode was fed with either $H_2$ or $H_2$/100 ppm CO, repeating the process several times, whereas the cathode was constantly fed with $O_2$, keeping the cell at the condition of open circuit potential.

Cyclic voltammetry was applied to the single cell electrodes to investigate the effect of potential cycling and its use as degradation testing technique [23,24]. In these experiments the anode, used as the working electrode, was exposed to Ar, and the cathode, used as the reference and counter electrodes, was exposed to $H_2$. The anode potential was cycled between 0.1 and 0.7 V, at a scan rate of 50 $mVs^{-1}$, at room temperature, up to a total of 5000 cycles. The performance of the MEAs was evaluated before the cycling process and at various stages of the cycling process, by measuring polarization and power density curves and anode overpotentials due to the presence of CO ($\eta_{CO}$) at a current density of 1 $Acm^{-2}$. These anode overpotentials were calculated as differences between the cell potentials in the presence and absence of CO (i.e., with the anode fed with $H_2$ + 100 ppm CO and pure $H_2$, respectively). Cyclic voltammetry was also applied to the cathode by the same procedure as for the anode, before the cycling process and then after the above-mentioned 5000 potential cycles.

## 3. Results and Discussions

### 3.1. Physical Characterization of the Electrocatalysts

The results of elemental analysis obtained by EDS are given in Table 1. The corresponding EDS spectra are shown in Fig. 1. A molybdenum content of only 19 wt% was obtained for the $Mo_2C$/C (30 wt%) support. The measured Pt and PtMo loadings (for the Pt/$Mo_2C$/C, PtMo/$Mo_2C$/C and PtMo/C electrocatalysts) resulted less than the target value of 20 wt%. It should be noted that the total Mo content of the PtMo/$Mo_2C$/C catalyst has contributions from the carbide and from the bimetallic particles. A small reduction in the Mo content of $Mo_2C$/C was observed after the addition of Pt and PtMo, which could be due to a partial dissolution of Mo during the deposition process. Surface areas of $Mo_2C$/C support and Pt/$Mo_2C$/C, PtMo/$Mo_2C$/C and PtMo/C electrocatalysts, determined by BET gas adsorption isotherms, are included in Table 1. A decrease in the overall surface area was observed for Pt/$Mo_2C$/C and PtMo/$Mo_2C$/C, which may be due to blocking of the pores by Pt and PtMo nanoparticles. Fig. 2 presents the X-ray diffraction patterns obtained for $Mo_2C$/C, Pt/$Mo_2C$/C, PtMo/$Mo_2C$/C and PtMo/C electrocatalysts. The pattern of $Mo_2C$/C presents peaks of both α-$Mo_2C$ and β-$Mo_2C$ [25,26], whereas that of Pt/$Mo_2C$/C, PtMo/$Mo_2C$/C and

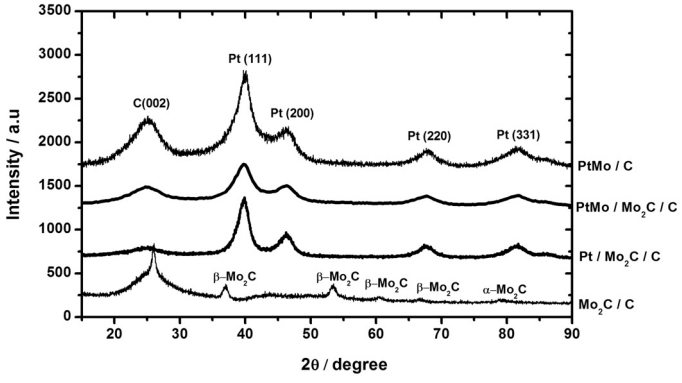


**Fig. 2.** X-ray diffraction patterns of the $Mo_2C$/C support and the Pt/$Mo_2C$/C, PtMo/$Mo_2C$/C and PtMo/C electrocatalysts.

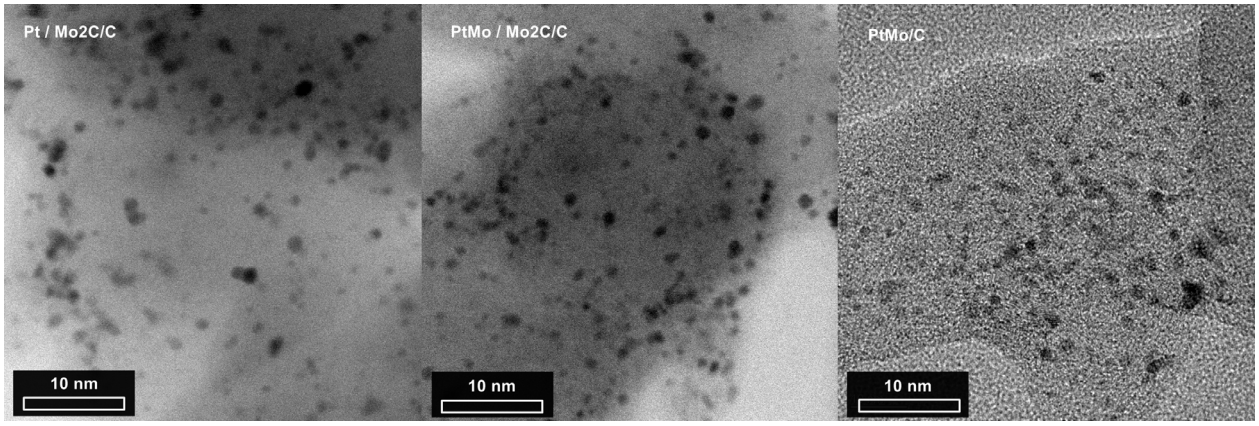


**Fig. 3.** TEM images of the Pt/$Mo_2C$/C, PtMo/$Mo_2C$/C, and PtMo/C electrocatalysts.

PtMo/C predominantly exhibit the peaks of the crystalline structure of Pt.

These results of XRD are consistent to the already reported data [26], where the $Mo_2C$ peaks disappeared after the addition of Pt to the $Mo_2C$/CNTs support. As only Pt peaks appeared in the XRD pattern of Pt-$Mo_2C$/CNTs, the authors explained that due to small differences in the crystal lattice spacing of Pt and $Mo_2C$, it is difficult to distinguish the Pt and $Mo_2C$ peaks. It is worth mentioning that significant contents of molybdenum in the samples were detected by EDS, despite the fact that almost no molybdenum crystalline phases were detected by XRD. The average Pt crystallite sizes calculated for these catalysts are given in Table 1. The values of lattice parameters (Table 1) indicate no inclusion of Mo in the Pt crystallites.

Fig. 3 shows typical TEM images of the Pt/$Mo_2C$/C, PtMo/$Mo_2C$/C and PtMo/C catalysts. The average particle diameters measured from these images are consistent with the mean crystallite sizes calculated from the XRD patterns, as can be seen in Table 1. A clear difference between the carbon black and molybdenum carbide supports can be observed from these TEM images. Quite uniform dispersion of Pt and PtMo particles were obtained for all catalysts. The effect of $Mo_2C$ and Mo on the occupancy of d electronic states in Pt atoms of the catalysts was investigated by measuring XANES spectra at the Pt $L_3$ edge. The X-ray absorption at the Pt $L_3$ edge corresponds to $2p_{3/2}$-5d electronic transitions and the magnitude of the white line is directly related to the occupancy of 5d electronic states. Differences in XANES spectra or in white line intensities are mainly related to differences in the electronic properties (the oxidation state) of the absorbing atom due to the electron donating or withdrawing properties of the neighboring atoms. An increase in white line intensity indicates an increase in the number of vacancies [27–29].

Fig. 4 shows XANES spectra of the PtMo/$Mo_2C$/C, PtMo/C and Pt/C electrocatalysts, recorded at the Pt $L_3$ edge before and after the adsorption of CO with the electrodes polarized at 50 mV vs. RHE. A slight but consistent increase in the white line intensity of PtMo/$Mo_2C$/C and PtMo/C as compared to Pt/C, can be observed in the XANES spectra recorded in $H_2$ atmosphere (see the inset of Fig. 4a). This indicates that the presence of Mo or $Mo_2C$ near the Pt atom may induce a slight increase in the number of Pt 4d band vacancies by changing its chemical environment. Fig. 4b shows the XANES spectra recorded after the CO poisoning of the catalysts. As it can be seen, a noticeable increase of the white line intensities was produced by the CO adsorption in three electrocatalysts, as a result of electron back donation from Pt to CO (see the inset of Fig. 4b). Because the white line intensity of Pt/C is smaller than those of PtMo/$Mo_2C$/C and PtMo/C in the absence of CO, but the three white line intensities are similar in the presence of CO, the change

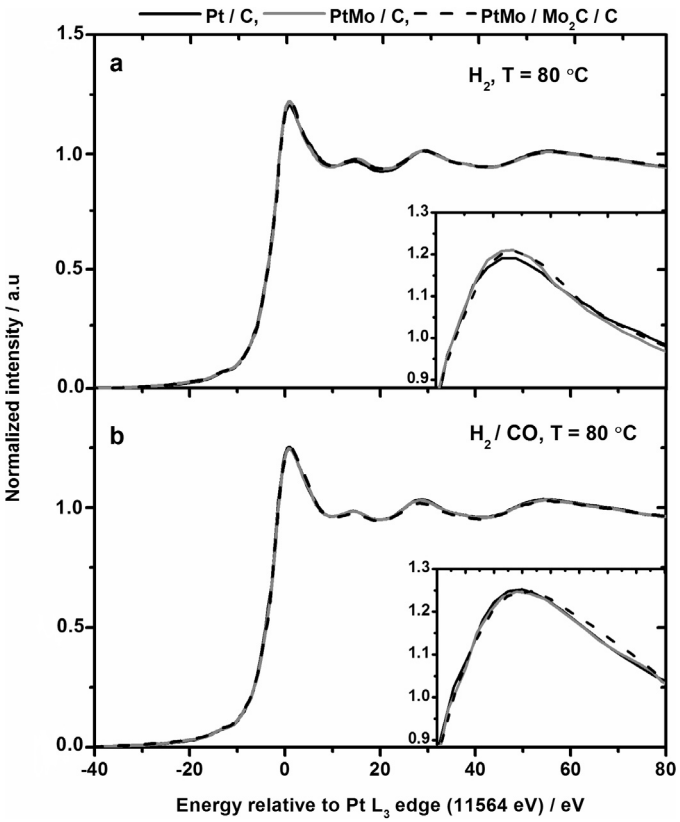


**Fig. 4.** XANES spectra at the Pt $L_3$ edge for the Pt/C, PtMo/C and PtMo/$Mo_2C$/C electrocatalysts exposed to $H_2$ (a) and $H_2$/CO (b) atmospheres.

caused by CO adsorption is greater for Pt/C than for PtMo/$Mo_2C$/C and PtMo/C catalysts, implying that more electrons are transferred from Pt to CO in the case of Pt/C. For Pt/C and PtMo/C electrocatalysts, the present results are in agreement with previously reported data [30,31].

### 3.2. Electrochemical characterization of the electrocatalysts

Figs. 5 and 6 show polarization and power density curves obtained for the Pt/C, Pt/$Mo_2C$/C, PtMo/C and PtMo/$Mo_2C$/C anodes, supplied with pure $H_2$ and $H_2$ containing 100 ppm CO, using Pt/C cathodes, supplied with $O_2$. These curves were recorded before the cycling process and after 1000, 3000 and 5000 potential cycles. As can be seen in Figs. 5b and 6a, Pt/$Mo_2C$/C and PtMo/$Mo_2C$/C showed the highest initial (0 cycle) hydrogen oxidation activity in the

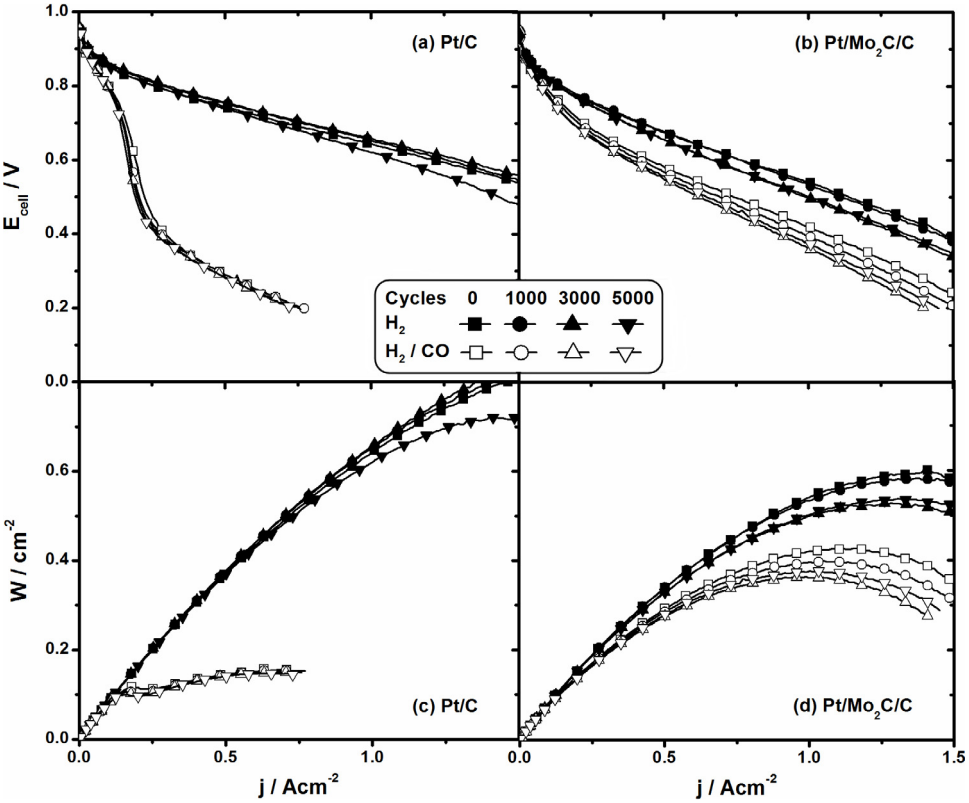


**Fig. 5.** PEM single cell polarization and power density curves measured at 85 °C with freshly prepared electrodes, and after 1000, 3000 and 5000 potential cycles. The Pt/C (a and c) and $Pt/Mo_2C/C$ (b and d) anodes were supplied with pure $H_2$ and $H_2$/100 ppm CO and the Pt/C cathodes were supplied with $O_2$.

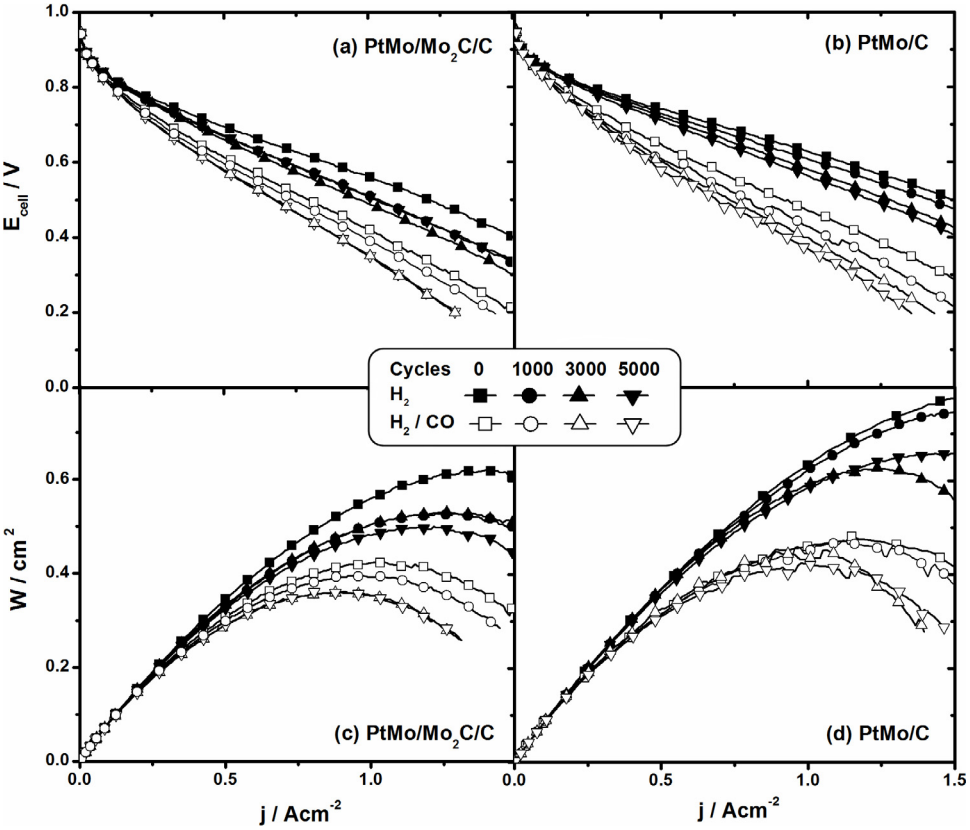


**Fig. 6.** PEM single cell polarization and power density curves measured at 85 °C with freshly prepared electrodes, and after 1000, 3000 and 5000 potential cycles. The $PtMo/Mo_2C/C$ (a and c) and PtMo/C (b and d) anodes were supplied with pure $H_2$ and $H_2$/100 ppm CO and the Pt/C cathodes were supplied with $O_2$.

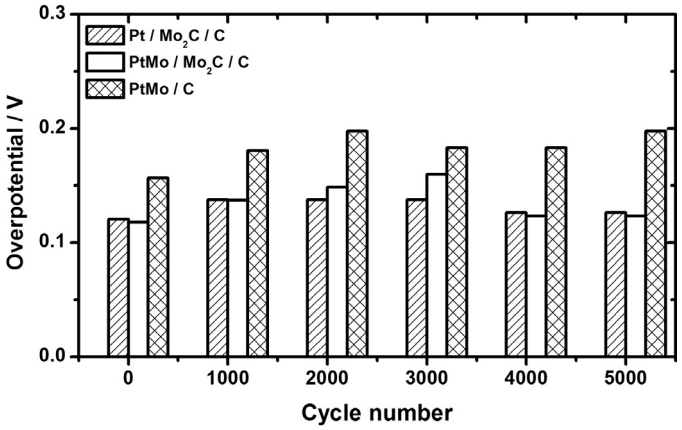


**Fig. 7.** Anode overpotential ($\eta_{CO}$) measured at 1 $Acm^{-2}$ prior the cycling process and after each 1000 potential cycles, for the $Pt/Mo_2C/C$, $PtMo/Mo_2C/C$ and PtMo/C catalysts.

presence of CO, giving CO induced overpotentials ($\eta_{CO}$) of ca. 120 mV for 1 $Acm^{-2}$ of current density, as compared to overpotential of 150 mV for PtMo/C, shown in Fig. 6b. On the other hand, for the Pt/C catalyst, the effect of CO poisoning is so adverse that the current density does not reach 1 $Acm^{-2}$ (see Fig. 5a). For Pt/C, a similar behavior can be observed in the power density curves, where the power density didn't reach 200 $mWcm^{-2}$ when the anode fuel is $H_2$ containing 100 ppm of CO (see Fig. 5c). On the other hand, the $Pt/Mo_2C/C$ catalyst yielded a power density of 400 $mWcm^{-2}$ in the presence of $H_2$/100 ppm CO, as shown in Fig. 5d. For the PtMo-based catalysts (Figs. 6c and 6d) high power densities were obtained for PtMo/C in the presence of both $H_2$ and $H_2$/100 ppm CO, but the decay of performance due to the cycling is much higher for PtMo/C than for $PtMo/Mo_2C/C$. The improved CO tolerance of the carbide-based electrocatalysts may be related to the efficiency of $Mo_2C/C$ to desorb or oxidize the adsorbed CO through a water-gas shift (WGS) reaction [5,9,32].

$$CO + H_2O \rightarrow CO_2 + H_2$$

After an initial decrease in the cell voltage, a quite constant cell performance was observed after around 1000 cycles, both in the presence and absence of CO, by the $Pt/Mo_2C/C$ and $PtMo/Mo_2C/C$ electrocatalysts (see Figs. 5b, and 6a). On the other hand for PtMo/C, the MEA performance in the presence of $H_2$ or $H_2$ containing CO deteriorates continuously with the cycling process, as can be observed in Fig. 6b. This can be due to a greater dissolution of Mo from the PtMo/C anode and its migration through the electrolyte membrane towards the cathode. When the catalyst support is molybdenum carbide, not only there is an increase in the oxidation of adsorbed CO, but also the electrocatalysts are more stable, as can be deduced from the polarization measurements. Results for the Pt/C anode show a stable performance of the MEA up to 5000 potential cycles in the presence of both $H_2$ and $H_2$/100 ppm CO, as can be observed in Fig. 5a, which is in agreement with previous results, where a better stability was obtained for the Pt electrocatalysts in comparison with Pt-M (M = second metal) electrocatalysts in PEMFCs [33].

Fig. 7 shows a comparison between the anode overpotentials with the electrocatalysts, before the cycling process and after each 1000 cycles, for a current density of 1 $Acm^{-2}$. A very little variation in the anode overpotential of $Pt/Mo_2C/C$ can be observed, reaching an almost constant value after 1000 cycles, whereas, the overpotentials of $PtMo/Mo_2C/C$ increase in the first 2000/3000 cycles and then decrease, reaching fairly constant values after 4000 cycles. On the other hand the overpotentials of PtMo/C remain variable during all the cycling process. The results of anodic overpotentials show

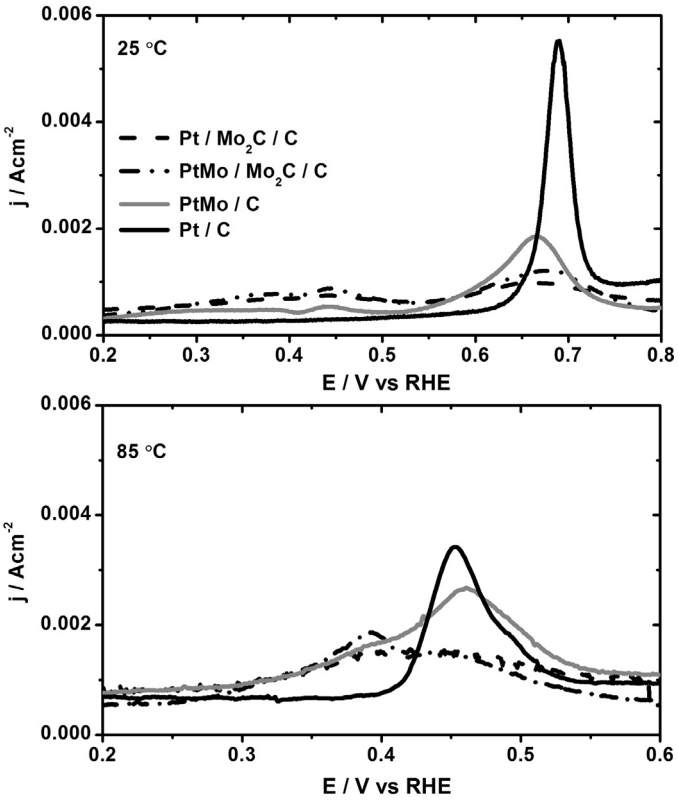


**Fig. 8.** CO stripping curves for the anodes formed by $Pt/Mo_2C/C$, $PtMo/Mo_2C/C$, PtMo/C and Pt/C electrocatalysts, measured at 25 °C (above) and 85 °C (below).

that the cell performance can be significantly improved by using Pt or PtMo supported on $Mo_2C/C$ as anode electrocatalysts, instead of using PtMo supported on carbon, as it is suggested by the values of overpotentials obtained after 4000/5000 cycles.

Fig. 8 shows the CO stripping profiles of $Pt/Mo_2C/C$, $PtMo/Mo_2C/C$, PtMo/C and Pt/C electrocatalysts, measured at 25 and 85 °C. At 25 °C, the profiles of $Pt/Mo_2C/C$, $PtMo/Mo_2C/C$ and PtMo/C exhibit CO electrooxidation peaks at about the same potential (0.665 V), meaning that at room temperature these three electrocatalysts have practically the same ability to oxidize the CO. For the Pt/C catalyst the CO electrooxidation occurs at a higher potential, indicating a poorer CO tolerance as compared to the other electrocatalysts, as also evidenced by polarization measurements. For the $Pt/Mo_2C/C$, $PtMo/Mo_2C/C$ and PtMo/C catalysts, part of CO is adsorbed on the Pt surface and part is directly oxidized to $CO_2$ (see Fig. 9) whereas for Pt/C catalyst, the only process is the adsorption on the catalyst surface. This explains why the CO stripping currents are larger for the Pt/C catalyst. These results are in agreement with previously reported data [12], where the CO oxidation shows a shift of 65 mV vs RHE towards more negative potentials for Pt/MoC/C in comparison to Pt/C. An increase in the temperature induces a decrease in the CO oxidation potential of the two carbide-based electrocatalysts, therefore at higher temperatures the molybdenum carbide-based electrocatalysts are more effective for the CO oxidation than the PtMo/C electrocatalyst.

Fig. 9 shows the results of online mass spectrometry (OLMS), obtained with the anodes maintained at the condition of open circuit potential. It can be observed that $CO_2$ production takes place when the anode is fed with $H_2$/100 ppm CO for the three catalysts, which evidences the oxidation of CO through a WGS reaction on the surface of the electrocatalysts [34]. There are some

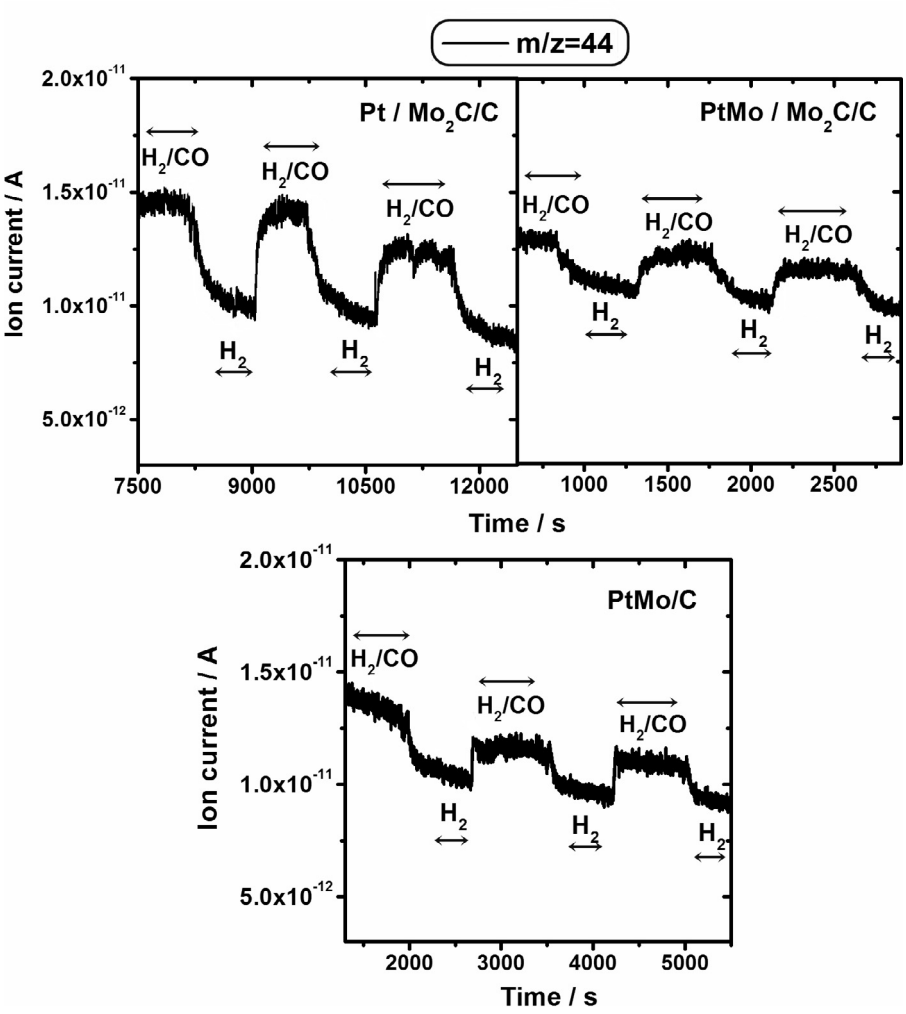


**Fig. 9.** Ion current obtained by OLMS with m/z = 44 for the Pt/$Mo_2C$/C, PtMo/$Mo_2C$/C and PtMo/C anodes supplied with pure $H_2$ or $H_2$/100 ppm CO. Cathodes formed by Pt/C were supplied with $O_2$.

differences in the extent of the $CO_2$ production, but this could be due to oscillations of the spectrometer response.

### 3.3. Degradation of the electrocatalysts

Figs. 10 and 11 show the cyclic voltammograms of the Pt/C, Pt/$Mo_2C$/C, PtMo/C and PtMo/$Mo_2C$/C electrocatalysts, measured before the cycling process and after 1000, 3000 and 5000 cycles. Besides the Pt-H desorption and adsorption peaks, an oxidation peak can be observed at ca. 0.45 V vs. RHE in the positive-going scan, for all the catalysts except Pt/C, and a relatively broad peak can be seen at 0.42 V vs. RHE in the negative-going scan, in the voltammetric profiles of the Mo-based electrocatalysts. This redox couple is in agreement with data from the literature and corresponds to an oxidation/reduction couple of $Mo^{+4}$ into $Mo^{+6}$ [30,31,35].

In all electrocatalysts except Pt/C a decrease in the peaks related to the oxidation/reduction reactions of Mo is noticeable after the potential cycling, which suggests that a partial dissolution of Mo species takes place in the acidic environment of the cell [36,37]. Nevertheless, for Pt/$Mo_2C$/C (Fig. 10b) and PtMo/$Mo_2C$/C (Fig. 11b) electrocatalysts the current densities and peak positions practically remain constant after 1000 potential cycles, suggesting that after an initial dissolution of some Mo species, no further dissolution takes place. On the other hand, the PtMo/C (Fig. 11a) suffers a gradual decrease in the current density and peak position during all the cycling process. This indicates that in spite of dissolution of some Mo species from $Mo_2C$/C support in PtMo/$Mo_2C$/C, the total dissolution of Mo is lower in PtMo/$Mo_2C$/C than in PtMo/C. These results are in agreement with the polarization measurements, where smaller variations in the anode overpotentials were observed for the Pt/$Mo_2C$/C and PtMo/$Mo_2C$/C electrocatalysts. Thus, the molybdenum carbide not only attenuates the CO poisoning, but also provides stability to the electrocatalysts, through the stabilization of the metal nanoparticles.

The dissolution of Mo species from the anode electrocatalysts and their migration towards the Pt/C cathodes were confirmed by cyclic voltammetry applied to the single cell cathodes, which was conducted initially after polarization measurements and then after 5000 potential cycles of the anode. As depicted in Fig. 12, a peak at 0.45 V vs. RHE in the positive-going scan can be observed in all the voltammograms, (except for the cell with the Pt/C anodic catalyst, Fig. 12a), i.e located at the same potential as in the voltammetric profile of the anode. This evidences the migration of Mo from the anode to the cathode, through the electrolyte membrane. Initially the intensities of Mo peaks in the Pt/C cathodes are weaker than those in the Pt/$Mo_2C$/C, PtMo/$Mo_2C$/C and PtMo/C anodes, but the corresponding peaks became sharper with the cycling process. Finally, in all cases, the intensities of Mo peaks in the anode and cathode voltammograms became similar after 5000 potential cycles, even though these intensities were different for the different

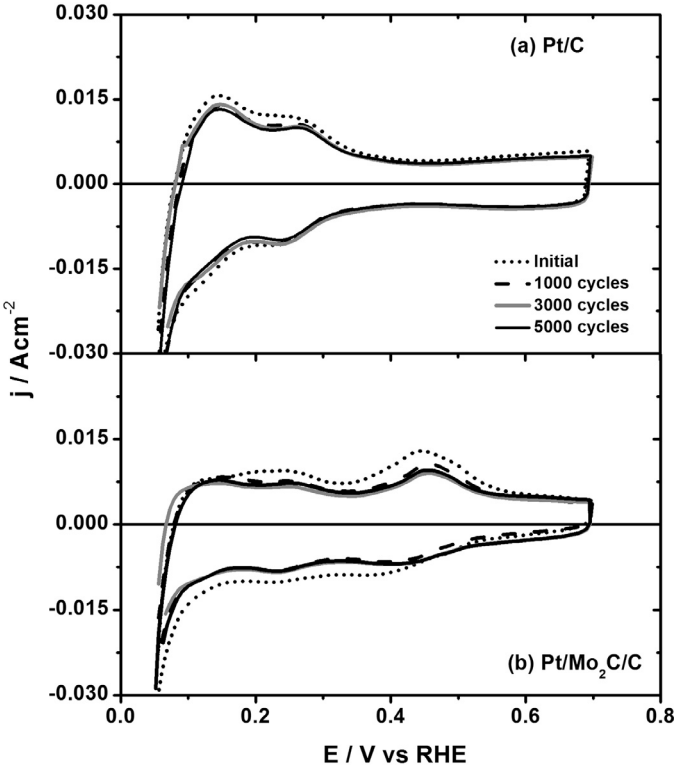


**Fig. 10.** Cyclic voltammograms of the anodes composed of Pt/C (a) and $Pt/Mo_2C/C$ (b), measured before the cycling process and after 1000, 3000 and 5000 potential cycles.

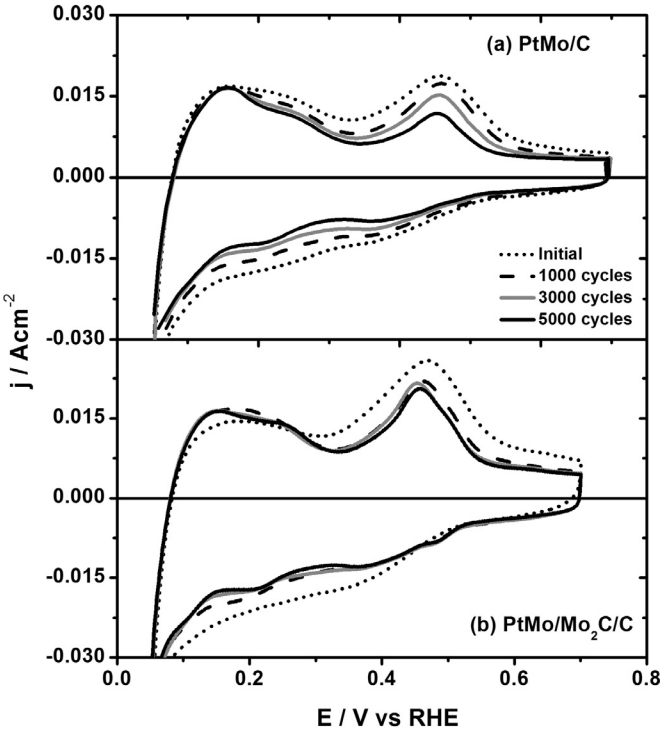


**Fig. 11.** Cyclic voltammograms of the anodes composed of PtMo/C (a) and $PtMo/Mo_2C/C$ (b) measured before the cycling process and after 1000, 3000, 5000 potential cycles.

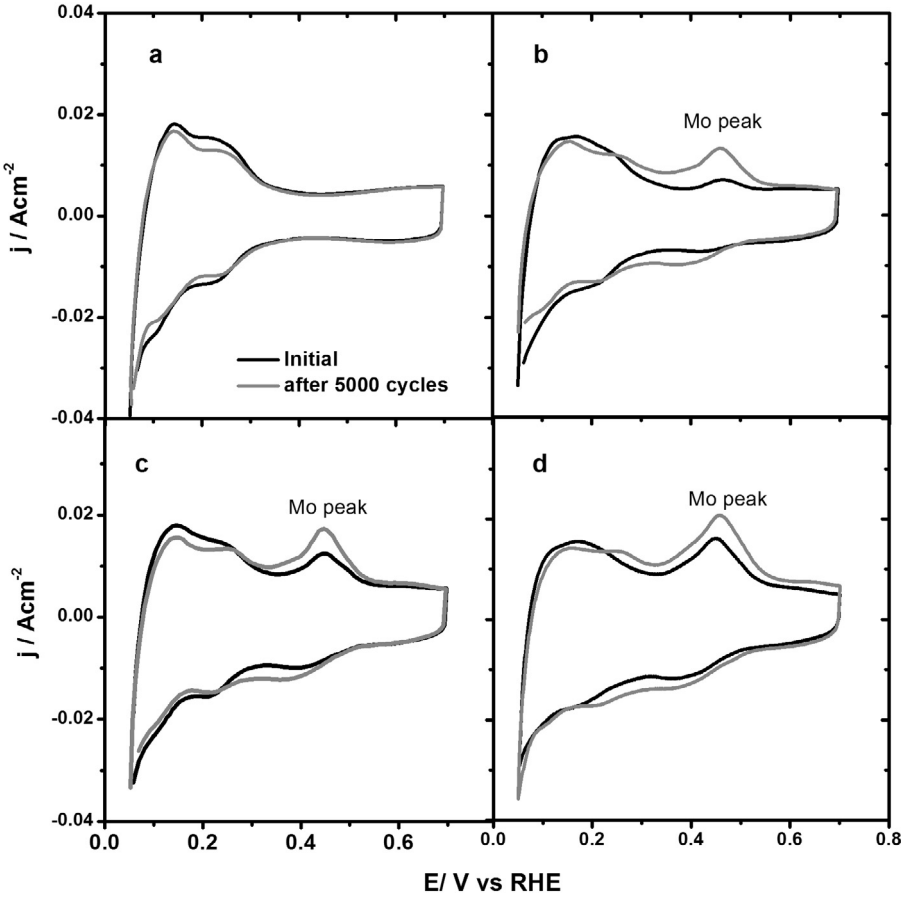


**Fig. 12.** Cyclic voltammograms of the Pt/C cathodes measured initially after polarization measurements and then after 5000 potential cycles of the Pt/C (a) $Pt/Mo_2C/C$ (b), PtMo/C (c) and $PtMo/Mo_2C/C$ (d) anodes.

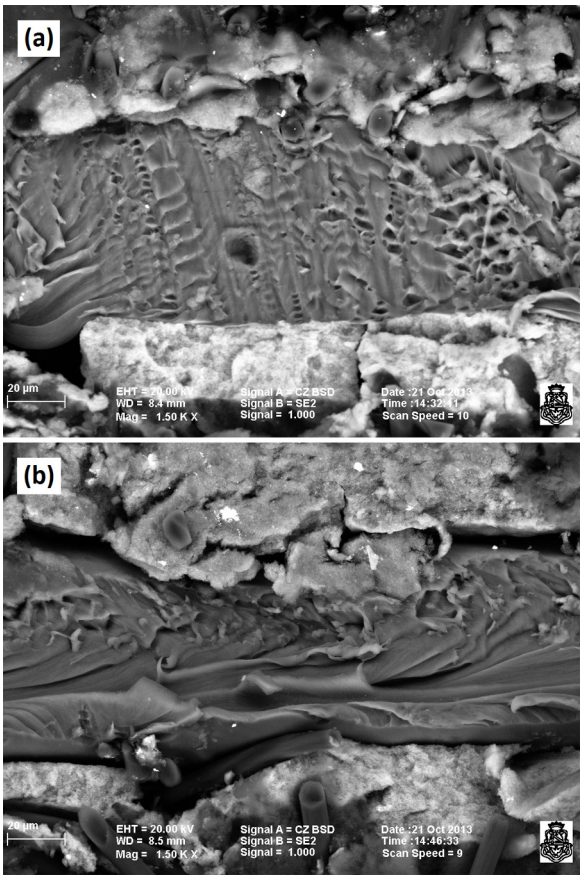


**Fig. 13.** Scanning electron micrographs of cross sections of the MEA composed of PtMo/$Mo_2C$/C in the anode and Pt/C in the cathode, recorded before (a) and after (b) the cycling process.

catalysts. These results are in agreement with previously reported data [30].

Scanning electron microscopy and x-ray analysis were performed in cross sections of new and cycled MEAs, in order to further investigate the migration of Mo species. As an example, Figs. 13a and 13b show micrographs of the MEA composed by PtMo/$Mo_2C$/C in the anode and Pt/C in the cathode, recorded with backscattered electrons, before and after the cycling process, respectively. All the components of the MEA, such as the carbon cloth, the gas-diffusion electrodes and the electrolyte membrane, can be easily identified in these micrographs. Some signs of deterioration can be appreciated in the cycled MEA (Fig. 13b), such as the presence of fractures in the gas-diffusion electrodes and detachments from the membrane. Similar features were observed in the micrographs of the other MEAs. The brightness of the catalyst layers is due to the presence of metal nanoparticles.

Fig. 14 shows x-ray spectra of the Pt/C cathodes of the MEAs composed by PtMo/$Mo_2C$/C and PtMo/C in the anode, recorded before and after the cycling process, with a 20 keV incident electron beam and a wavelength dispersive spectrometer, in the energy range between 2.28 and 2.35 keV. As it can be seen, the S-K$\alpha_{1,2}$ and S-K$\alpha_{3,4}$ peaks are present in all the spectra, which is due to the sulfur content of the Nafion. The Pt-M$\gamma$ peak is also present in all the spectra, which is due the platinum content of the Pt/C cathode catalysts. The presence of these peaks in the spectra is to be expected. Regarding the molybdenum, it was detected only in the cathodes of the cycled MEAs, as manifested by the Mo-L$\alpha_{1,2}$ peak. This fact is in agreement with the results of the cyclic voltammetry performed to the Pt/C cathodes. During the cycling process, the Mo is partially dissolved from the anode, passes through the membrane, and reaches

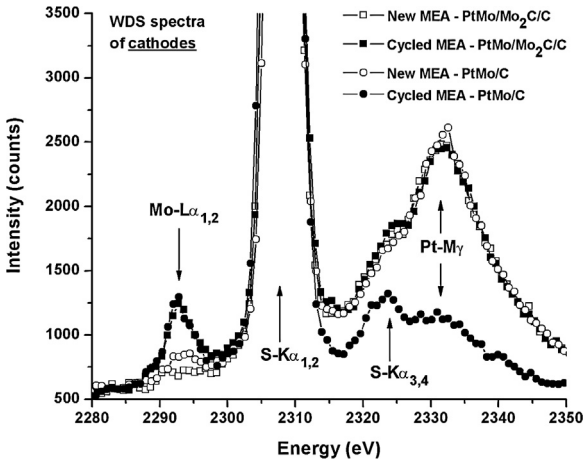


**Fig. 14.** WDS spectra of the Pt/C cathodes of new and cycled MEAs composed of PtMo/$Mo_2C$/C and PtMo/C in the anodes.

the cathode, as it was previously discussed. It is worth mentioning that, a small amount of Mo can also be appreciated in the cathodes of the new MEAs, but in these cases, the presence of Mo is due to a contamination produced by the transversal cut of the MEAs during the sample preparation.

The molybdenum species that reach the cathode interfere not only with the kinetics of oxygen reduction reaction (ORR) in the cathode, but also with the conduction of protons through the electrolyte membrane. Therefore the ORR, which itself is a kinetically slow process, is further slowed down by the presence of Mo ionic species, thus having a negative effect on the MEA performance. However, as seen previously, the use of molybdenum carbide support for the anode electrocatalyst can effectively control the loss of Mo species, helping to keep the CO tolerance. The molybdenum carbide not only provides stability, but also enhances the CO tolerance of the anode electrocatalyst.

## 4. Conclusions

The activity, stability and CO tolerance of molybdenum carbide-based electrocatalysts were studied in PEMFC anodes. Physical and electrochemical properties of Pt/$Mo_2C$/C, PtMo/$Mo_2C$/C, PtMo/C and Pt/C electrocatalysts were analyzed, at several stages of a cycling process performed in typical working conditions. It was observed that the partially carburized Pt/$Mo_2C$/C and PtMo/$Mo_2C$/C electrocatalysts, resulted in a higher activity for the hydrogen oxidation reaction in the presence of 100 ppm of carbon monoxide, as compared to PtMo/C. In addition, degradation analyses showed that the carbide-based electrocatalysts are significantly more stable than PtMo/C. The good stability and excellent electrocatalytic activity for hydrogen oxidation can be attributed to the high oxidation resistance of $Mo_2C$/C and to its significant interaction with metal and alloy particles. Polarization measurements and cyclic voltammetric results suggest that $Mo_2C$/C can be considered as a promising electrocatalyst support to improve the performance and durability of Mo-based anodes in proton exchange membrane fuel cells.

## Acknowledgment

The authors would like to thank the Third World Academy of Science (TWAS), Italy, the Conselho Nacional de Desenvolvimento Científico e Tecnológico (CNPq), Fundação de Amparo à Pesquisa do Estado de São Paulo, Brazil and the Secretaría de Ciencia y Técnica (SeCyT) of the Universidad Nacional de Córdoba (UNC), Argentina,

for financial supports, and the Brazilian Synchrotron Light Laboratory (LNLS), Brazil where XAS measurements were performed.

## References

[1] J. Kunze, U. Stimming, Electrochemical versus heat-engine energy technology: a tribute to Wilhelm Ostwald's visionary statements, Angewandte Chemie International Edition 48 (2009) 9230.
[2] J.J. Baschuk, X. Li, Carbon monoxide poisoning of proton exchange membrane fuel cells, International Journal of Energy Research 25 (2001) 695.
[3] F. Hajbolouri, B. Andreaus, G.G. Scherer, A. Wokaun, CO Tolerance of commercial Pt and PtRu gas diffusion electrodes in polymer electrolyte fuel cells, Fuel Cells; From Fundamentals to Systems 4 (2004) 160.
[4] H. Yu, Z. Hou, B. Yi, Z. Lin, Composite anode for CO tolerance proton exchange membrane fuel cell, Journal of Power Sources 105 (2002) 52.
[5] J. Patt, D.J. Moon, C. Phillips, L. Thompson, Molybdenum carbide catalysts for water–gas shift, Catalysis Letter 65 (2000) 193.
[6] A. Celzard, J.F. Marêché, G. Furdin, V. Fierro, C. Sayag, J. Pielaszek, Preparation and catalytic activity of active carbon-supported $Mo_2C$ nanoparticles, Green Chemistry 7 (2005) 784.
[7] S.T. Oyama, Preparation and catalytic properties of transition metal carbides and nitrides, Catalysis Today 15 (1992) 179.
[8] R.B. Levy, M. Boudart, The kinetics and mechanism of spillover, Journal of Catalysis 32 (1974) 304.
[9] E.C. Weigert, N.A. Smith, B.G. Willis, A. Amorelli, J.G. Chen, PVD synthesis and characterization of Pt-modified molybdenum carbides as potential electrocatalysts, Electrochemical and Solid-State Letters 8 (2005) A337.
[10] T. Matsumoto, T. Komatsu, H. Nakano, K. Arai, Y. Nagashima, E. Yoo, T. Yamazaki, M. Kijima, H. Shimizu, Y. Takasawa, J. Nakamura, Efficient usage of highly dispersed Pt on carbon nanotubes for electrode catalysts of polymer electrolyte fuel cells, Catalysis Today 90 (2004) 277.
[11] P. Heo, M. Nagao, M. Sano, T. Hibino, A high-performance $Mo_2C$-$ZrO_2$ anode catalyst for intermediate-temperature fuel cells, Journal of the Electrochemical Society 154 (2007) B53.
[12] O. Guillén-Villafuerte, R. Guil-Lopez, E. Nieto, G. García, J.L. Rodríguez, E. Pastor, J.L.G. Fierro, Electrocatalytic performance of different Mo-phases obtained during the preparation of innovative Pt-MoC catalysts for DMFC anode, International Journal of Hydrogen Energy 37 (2012) 7171.
[13] E.C. Weigert, D.V. Esposito, J.G. Chen, Cyclic voltammetry and X-ray photoelectron spectroscopy studies of electrochemical stability of clean and Pt-modified tungsten and molybdenum carbide (WC and $Mo_2C$) electrocatalysts, Journal of Power Sources 193 (2009) 501.
[14] T. Hyeon, M. Fang, K.S. Suslick, Nanostructured molybdenum carbide: Sonochemical synthesis and catalytic properties, Journal of American Chemical Society 118 (1996) 5492.
[15] K.S. Suslick, T. Hyeon, M. Fang, Nanostructured materials generated by high-intensity ultrasound: Sonochemical synthesis and catalytic studies, Chemistry of Materials 8 (1996) 2172.
[16] L.G.S. Pereira, V.A. Paganin, E.A. Ticianelli, Investigation of the CO tolerance mechanism at several Pt-based bimetallic anode electrocatalysts in a PEM fuel cell, Electrochimica Acta 54 (2009) 1992.
[17] E.I. Santiago, V.A. Paganin, M. Carmo, E.R. Gonzalez, E.A. Ticianelli, Studies of CO tolerance on modified gas diffusion electrodes containing ruthenium dispersed on carbon, Journal of Electroanalytical Chemistry 575 (2005) 53.
[18] G.A. Camara, M.J. Giz, V.A. Paganin, E.A. Ticianelli, Correlation of electrochemical and physical properties of PtRu alloy electrocatalysts for PEM fuel cells, Journal of Electroanalytical Chemistry 537 (2002) 21.
[19] V. Radmilovic, H.A. Gasteiger, P.N. Rose, Structure and chemical composition of a supported Pt-Ru electrocatalyst for methanol oxidation, Journal of Catalysis 154 (1995) 98.
[20] L.G.S. Pereira, F.R. Santos, M.E. Pereira, V.A. Paganin, E.A. Ticianelli, CO tolerance effects of tungsten-based PEMFC anodes, Electrochimica Acta 51 (2006) 4061.
[21] A.C. Garcia, V.A. Paganin, E.A. Ticianelli, CO tolerance of PdPt/C and PdPtRu/C anodes for PEMFC, Electrochimica Acta 53 (2008) 4309.
[22] E.I. Santiago, G.A. Camara, E.A. Ticianelli, CO tolerance on PtMo/C electrocatalysts prepared by the formic acid method, Electrochimica Acta 48 (2003) 3527.
[23] S. Zhang, X. Yuan, J.N.C. Hin, H. Wang, K.A. Friedrich, M. Schulze, A review of platinum-based catalyst layer degradation in proton exchange membrane fuel cells, Journal of Power Sources 194 (2009) 588.
[24] R.L. Borup, J.R. Davey, F.H. Garzon, D.L. Wood, M.A. Inbody, PEM fuel cell electrocatalyst durability measurements, Journal of Power Sources 163 (2006) 76.
[25] J.A. Schaidle, N.M. Schweitzer, O.T. Ajenifujah, L.T. Thompson, On the preparation of molybdenum carbide-supported metal catalysts, Journal of Catalysis 289 (2012) 210.
[26] M. Pang, C. Li, L. Ding, J. Zhang, D. Su, W. Li, C. Liang, Microwave-assisted preparation of $Mo_2C$/CNTs nanocomposites as efficient electrocatalyst supports for oxygen reduction reaction, Industrial and Engineering Chemistry Research 49 (2010) 4169.
[27] A.E. Russell, A. Rose, X-ray absorption spectroscopy of low temperature fuel cell catalysts, Chemical Reviews 104 (2004) 4613.
[28] J.H. Bang, H. Kim, CO-tolerant PtMo/C fuel cell catalyst for $H_2$ oxidation, Bulletin of Korean Chemical Society 32 (2011) 3660.
[29] A. Witkowska, E. Principi, A. Di Cicco, S. Dsoke, R. Marassi, L. Olivi, M. Centazzo, V.R. Albertini, Temperature and potential-dependent structural changes in a Pt cathode electrocatalyst viewed by in situ XAFS, Journal of Non-Crystalline Solids 354 (2008) 4227.
[30] T.C.M. Nepel, P.P. Lopes, V.A. Paganin, E.A. Ticianelli, CO tolerance of proton exchange membrane fuel cells with Pt/C and PtMo/C anodes operating at high temperatures: A mass spectrometry investigation, Electrochimica Acta 88 (2013) 217.
[31] A. Hassan, A. Carreras, J. Trincavelli, E.A. Ticianelli, Effect of heat treatment on the activity and stability of carbon-supported PtMo alloy electrocatalysts for hydrogen oxidation in proton exchange membrane fuel cells, Journal of Power Sources 247 (2014) 712.
[32] J.A. Schaidle, A.C. Lausche, L.T. Thompson, Effects of sulfur on $Mo_2C$ and Pt/$Mo_2C$ catalysts: Water gas shift reaction, Journal of Catalysis 272 (2010) 235.
[33] O.T. Holton, J.W. Stevenson, The role of platinum in proton exchange membrane fuel cells, Platinum Metals Review 57 (2013) 259.
[34] A. Manasilp, E. Gulari, Selective CO oxidation over;1; Pt/alumina catalysts for fuel cell applications, Applied Catalysis B: Environmental 37 (2002) 17.
[35] L.C. Ordóñez, P. Roquero, P.J. Sebastian, J. Ramírez, Carbon-supported platinum-molybdenum electro-catalysts for methanol oxidation, Catalysis Today 107 (2005) 46.
[36] N.P. Lebedeva, G.J.M. Janseen, On the preparation and stability of bimetallic PtMo/C anodes for proton-exchange membrane fuel cells, Journal of Electrochimica Acta 51 (2005) 29.
[37] S. Mukerjee, S.J. Lee, E.A. Ticianelli, J. McBreen, B.N. Grgur, N.M. Markovic, P.N. Ross, J.R. Giallombardo, E.S. De Castro, Investigation of enhanced CO tolerance in proton exchange membrane fuel cells by carbon supported PtMo alloy catalyst, Electrochemical and Solid-State Letters 2 (1999) 12.